Analytical Bistatic k Space Images Compared to Experimental Swept Frequency ISAR Images

John Shaeffer, Brett Cooper
Marietta Scientific, Inc.
376 Powder Springs St. 240A
Marietta, Georgia 30064
(770) 425-9760
www.inetnow.net/~msi

Kam Hom
NASA Langley Research Center
Hampton, Virginia 23681
(757) 864-5292
k.w.hom@larc.nasa.gov

ABSTRACT: A case study of flat plate scattering images obtained by the analytical bistatic k space and experimental swept frequency ISAR methods is presented. The key advantage of the bistatic k space image is that a single excitation is required, i.e., one frequency / one angle. This means that prediction approaches such as MOM only need to compute one solution at a single frequency. Bistatic image Fourier transform data are obtained by computing the scattered field at various bistatic positions about the body in k space. Experimental image Fourier transform data are obtained from the measured response to a bandwidth of frequencies over a target rotation range.

This paper compares both image approaches as applied to a flat plate. Full details are presented in [1].

Analytical and Experimental Images: Experimental images are the Fourier transform of the backscatter reflected field as a function of frequency and angle, $E(\omega,\theta)$. Analytical bistatic k space images [1] are the Fourier transform of the bistatic field computed from a current distribution **J** as a function of down and cross range wave number **k**, $E(\vec{k}_{down}, \vec{k}_{cross})$. This quantity is computed from a single current distribution **J**(ω) from the generalized radiation integral

$$E_{pol}(\vec{k}_{down}, \vec{k}_{cross}) = \iint \left(\hat{u}_{pol} \cdot J(\omega)\right) e^{j\vec{k}\cdot\vec{R}}\, dS \tag{1}$$

where the wave vector **k** takes on down and cross range values in k space,

$$\vec{k} = (\Delta k + k_0)\, \hat{k}_{down} + \Delta k\, \hat{k}_{cross},$$

where Δk is the k-space bandwidth in the down and cross range directions and $k_0 = 2\pi/\lambda$ is the nominal wave number corresponding to the excitation frequency ω. The resolution in each spatial direction is $\Delta r = 2\pi/\Delta k$ which can be recast in terms of fractional wave number space (similar to fractional frequency bandwidth), $\Delta r = \lambda/(\Delta k/k_0)$. Experimental resolution for comparison is $\Delta r = (\lambda/2)/(\Delta f/f_0)$ for downrange and $\Delta r = (\lambda/2)/(\Delta\theta)$ for cross range. The bistatic k-space bandwidth will be twice the experimental bandwidth for the same resolution Δr due to the bistatic one way path length change.

Table 1 compares various image issues between the experimental swept frequency ISAR approach and the analytical bistatic k-space approach.

Experimental and Bistatic k space image comparison: Due to space limitations, only 2-D cases are presented. The interested reader is directed to [1] for the 1-D cases. The target is a 6" (0.15 m) square plate viewed from three aspect angles: normal to the plate; edge on at 10° elevation; and at 45° azimuth along the diagonal at 10° elevation. The illumination frequency is 10 GHz with a wavelength of 1.18" (0.03 m). The normalized plate dimensions are $\ell/\lambda = 5.08$ and $A/\lambda^2 = 25.9$ for edge length and plate area respectively.

The analytical and experimental image comparisons each used a Hanning window function. The experimental data used a single resolution $\Delta r = 1.25\ \lambda$. The analytical images used three resolutions, which were 0.4, 0.8, and 1.2 times the Δr of the experimental value. This was done to demonstrate how resolution affects the resulting images.

The experimental resolution is $1.25\ \lambda_c = 1.47" = 0.0375$ m corresponding to a fractional bandwidth Δf/f of 0.4 (8-12GHz) and an ISAR rotation angle of 20°. The bistatic k space image resolutions were 1.5, 1.0, and 0.5 λ corresponding to

0.015, 0.030, and 0.045 m respectively. This bracketed the experimental value. The nominal bistatic viewing angles were 38°, 57°, and 115° respectively.

The data scales between the experimental and computed images have been kept the same.

Computational Parameters: The square plate bistatic k space images were computed using MOM3D [3]. The mesh model had 5000 triangles resulting in 7400 unknowns. The geometry symmetry option was utilized so that the system matrix was decomposed into two smaller matrices of 3725 and 3675 unknowns each. The sample density was 286 unknowns / λ^2. The image extent was set to 0.5 m.

Image Comparisons: *View 1* is perpendicular to the plate, Figure 1, for horizontal polarization. The dominant scattering for this case is specular with a peak RCS of $\sigma_{specular} = 4\pi \frac{A^2}{\lambda^2} = 7.6\ \mathrm{m}^2 = 8.8\ \mathrm{dBsm}$. The 2-D images show backscattered radiation to be uniformly coming from the entire plate. Coarser resolutions distribute energy over the larger resolution cell.

The experimental image shows a lower level source emanating from behind the plate probably due to edge to edge diffraction sometimes called talking edges. This return is in the category of a multiple bounce and hence images later in time down range of the plate. This effect is not seen in the computed images. Residual signal processing side lobes are seen in the computed 2-D images.

View 2 is normal to the plate edges at an elevation angle of 10°. The dominant scattering is due to edge diffraction: leading edge for horizontal (parallel) polarization, Figure 2; and trailing edge, or alternately traveling wave reflection for vertical (perpendicular) polarization, Figure 3.

The H pol images show the leading edge as the dominant scattering mechanism along with two edge waves reflecting from the rear vertices. The leading edge return, from the 1-D images, is close to the theoretical knife edge value of $\sigma_{edge} = \ell^2 / \pi = 0.0074\mathrm{m}^2 = -21.3\ \mathrm{dBsm}$. The experimental image also shows a scattering center behind the plate due to rear corner to corner diffraction that arrives later in time. The edge wave mechanism in the computed images shows a spatial distribution with a peak at the rear vertex. This corresponds to the interpretation that the edge wave, upon reflection, loses energy via radiation as it travels back towards the front corner. Thus we see in the image a decaying intensity. The coarser resolution computed images distribute the return over a larger spatial extent.

The V pol images show the trailing edge as the dominant scattering mechanism. The experimental image also shows a scattering center behind the plate due to a second bounce surface wave, i.e., from the rear edge to the front and a second reflection from the back edge. This arrives later in time and experimentally images behind the plate. This is not seen in the computed images.

The experimental V pol images suggest a scattering mechanism from the front edge of the plate which is not observed in the computed images. We believe this is due to the trailing edge reflected surface wave and that if the plate were electrically longer we would not see the leading edge. The computed images do not show a leading edge scattering center. The dominant mechanism for this viewing angle is the trailing edge traveling wave reflection. In the computed 1-D and 2-D images the peak occurs at the rear and decays towards the front of the plate. This corresponds to the interpretation that the traveling wave, upon reflection, loses energy via radiation as it travels back towards the front edge. Thus the image decays in intensity. This phenomenon is not observed in the experimental data because the swept frequency nature of the image causes the stationary phase locations to coincide with the edges of the plate. The leading edge return in the experimental images is interpreted as the trailing edge reflected surface wave that has not completely decayed by the time it reached the front. This happens because of the multiple bounce traveling wave arriving later in time. Because the traveling wave mechanism images differently for the computed and experimental approaches, the peak values do not correspond to each other.

View 3 is along the plate diagonal, azimuth angle of 45°, at an elevation angle of 10°, Figure 4 and 5 for H (parallel) and V (perpendicular) polarizations respectively. The dominant mechanisms are non-specular edge and traveling waves.

The H pol images show scattering from the four tips of the plate. The two dominant tips are the mid vertices which reflect the edge traveling wave. The 1.0 and 0.5 λ resolution images show these reflected edge waves on the two front illuminated edges with the peak amplitudes near the reflection point. The rear vertex scattering center is probably due to

edge waves that "turned the first corner" and then reflected from the rear most vertex and / or possibly due to tip diffraction since the plate is viewed at an elevation of 10°. The front tip return has the lower magnitude and is due to tip diffraction.

The experimental images show the front vertex with a lower amplitude than the rear. The opposite occurs in the computed images. The reason for this is not clear. It is conjectured that the measured front tip image is the phasor sum of tip diffraction and the remainder of the reflected edge wave which are phase subtracting to produce a smaller return.

The V pol images show scattering from the rear vertex and is due to the reflected surface traveling wave. As before with traveling wave mechanisms, the experimental and computed image magnitudes differ. The computed results show a lower amplitude spatially distributed return while the experimental image shows a higher amplitude return localized to the rear vertex. The computed images show the maximum amplitude near the aft reflection point with the reflected traveling wave decreasing in intensity as is propagates toward the front. The 1-D measured image shows a small return from the front tip which may be the stationary phase residual of the reflected traveling wave.

The view angle in elevation is less than the angle for maximum surface wave reflection which would occur, using the plate diagonal length, at about 18°.

Image comparison summary:

- Scattering mechanisms that are localized image similarly. The experimental and computed images are similar in most respects for specular and leading edge scattering. For trailing edge diffraction we suspect similar images; however, we have not made this comparison for a large λ target.

- Multiple bounce scattering mechanisms image differently. The experimental images show multiple reflections further down range since this is a time delay mechanism. This agrees with our physical view. The bistatic k space approach images the current distribution that by definition exists only on the surface and thus can not be further down range since there is no time variation. The computed images show multiple bounce mechanisms as locations on the body where those current mechanisms exist, i.e., placement of radar absorbing material at these locations would reduce the scattering.

- Surface traveling and edge waves image differently. (And we suspect for creeping wave mechanisms, although we have not made that comparison.) The computed images tend to show edge and traveling waves as distributed sources over the scattering surfaces/edges which corresponds to this physical mechanism. The swept frequency measured images show these mechanisms at the body fore and aft end point locations. In this case the bistatic images correspond closer to a physical view.

Summary: A bistatic k space imaging technique has been introduced which is applicable for many computational electromagnetic algorithms. Images are a useful diagnostic tool in that they provide a pictorial representation of those body currents which contribute to radiation in specified spatial directions. By knowing how the geometric current distribution radiates energy, it then becomes easier to modify the currents and/or geometry to produce user desired scattering or radiation results.

The bistatic k space image algorithm utilizes a computed body current distribution and a generalized k space radiation integral to compute the scattered field in k space. The Fourier transform of this data is then the image in one, two or three dimensions. This image technique can be applied to monostatic or bistatic scattering or to antennas since only one body excitation is required.

Bistatic k space images:

- *Bistatic k space images are not the same as experimental images.* Both methods produce similar results particularly for localized scattering mechanisms such as specular and edge diffraction. Experimental images show multiple bounce scattering centers delayed in time. Analytical k space images show the current distribution producing radiation. Surface traveling and edge waves image as distributed sources in the analytical k space method as compared to local end point regions in experimental images. Experimental images typically have two way path length changes while the bistatic k space images have a one way path length change.

- The method may be applied to any EM computational code that produces a current distribution, e.g., method of moments, physical optics, finite element frequency domain, etc. The computed current distribution must reside on the body, i.e., equivalent surface currents removed from the geometry will not image back to a physical source.

- The method is computationally cheap. It is equivalent to computing a bistatic or antenna radiation pattern from just one current excitation.

- Resolution is limited by the discreteness of the EM analysis and by user desired limits on the bistatic radiation angles.

- Image focusing and smearing is not a problem because the bistatic field is computed on a uniform grid in k space. Experimental data, in comparison, is usually on a circular arc region that must be projected to a uniform rectangular grid for input to an FFT.

- One, two or three-dimensional images may be obtained with a resolution limit of $\lambda/4$.

- The method may be used to produce images for antennas and for bistatic scattering or for monostatic scattering.

- Images may be made for arbitrary polarization, e.g., cross polarized images may be obtained.

References

1. John Shaeffer, Kam Hom, Craig Baucke, Brett Cooper, and Noel Talcott, Jr., "Bistatic k-Space Imaging for Electromagnetic Prediction Codes for Scattering and Antennas", NASA Technical Paper 3569, July 1996

2. John Shaeffer, Kam Hom, Craig Baucke, Brett Cooper, and Noel Talcott, Jr., "A Review of Bistatic k-Space Imaging for Electromagnetic Prediction Codes for Scattering and Antennas", IEEE Antennas and Propagation Magazine, Feature Article, vol. 39, no. 5, October, 1997.

3. John Shaeffer, "MOM3D Method of Moments Code Theory Manual," NASA CR 189594, Contract NAS1-18603, March 1992.

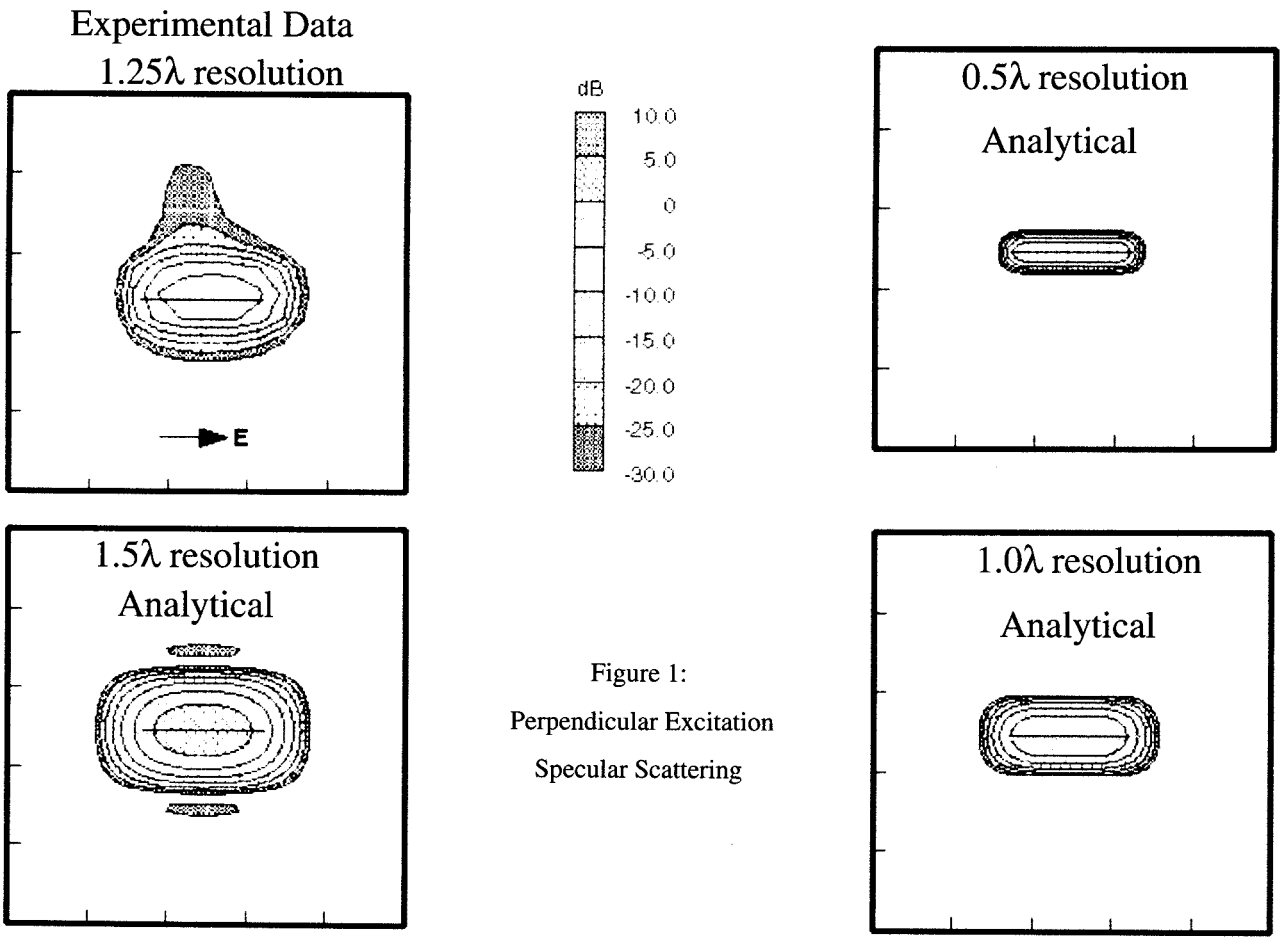

Figure 1:

Perpendicular Excitation

Specular Scattering

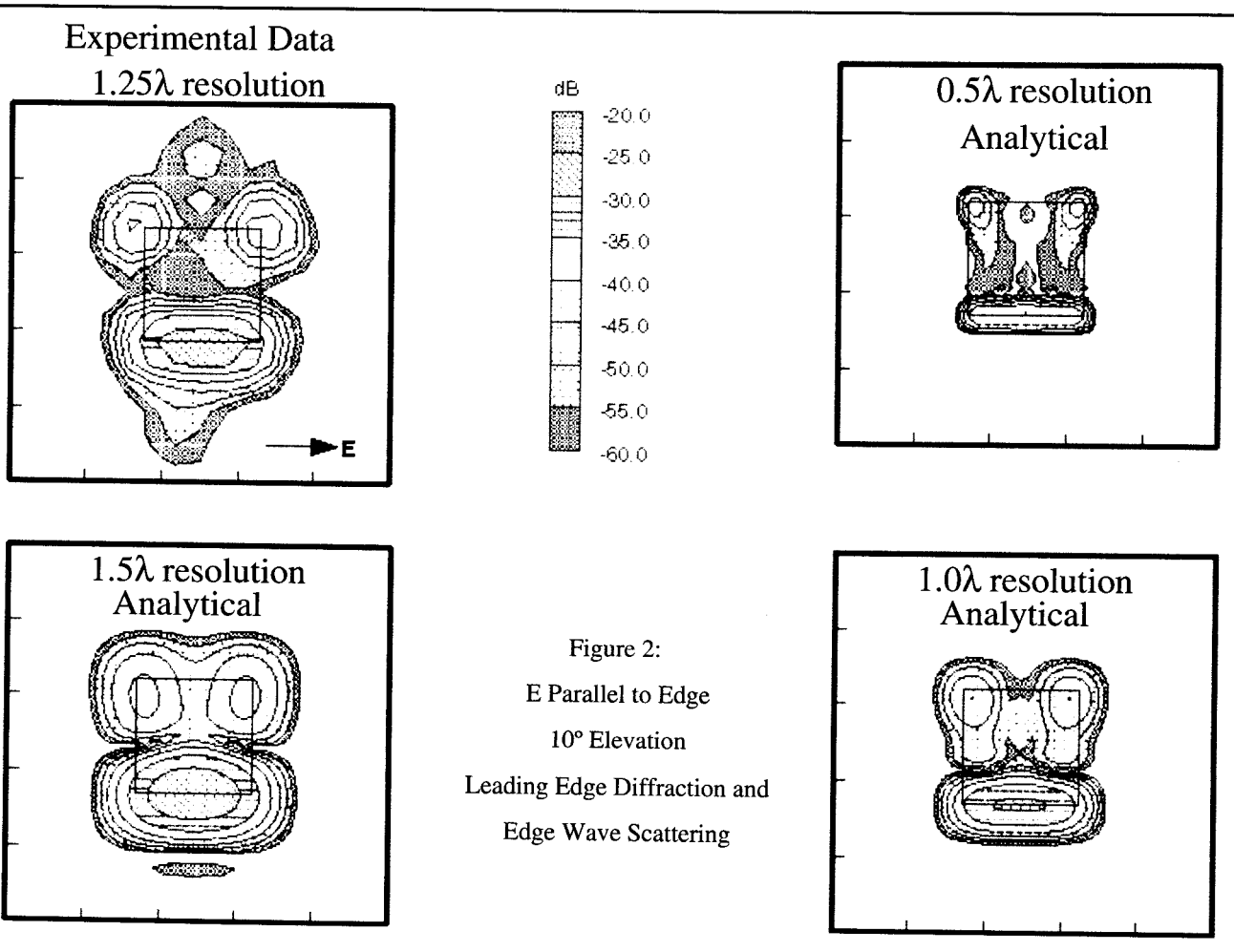

Figure 2:

E Parallel to Edge

10° Elevation

Leading Edge Diffraction and

Edge Wave Scattering

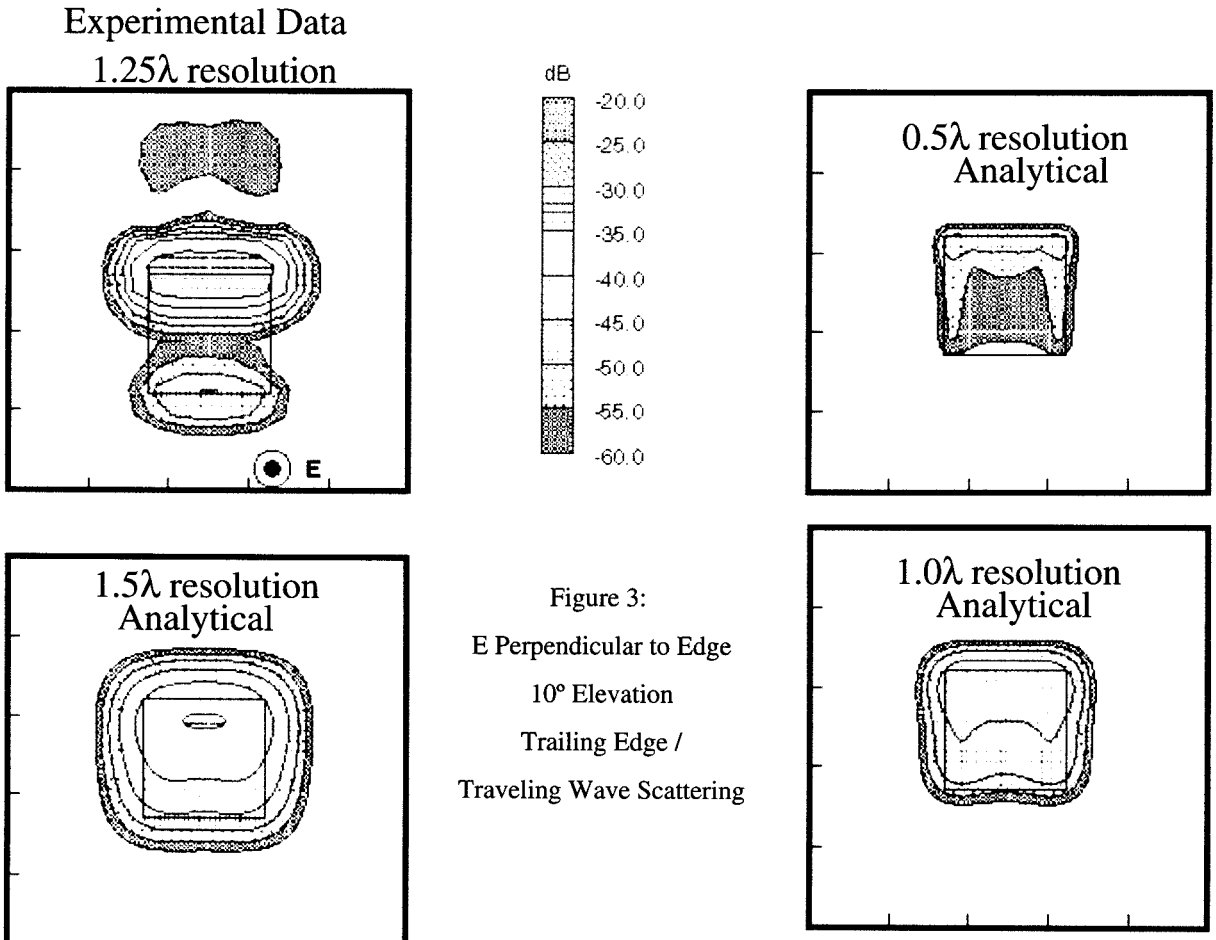

Figure 3:

E Perpendicular to Edge

10° Elevation

Trailing Edge /

Traveling Wave Scattering

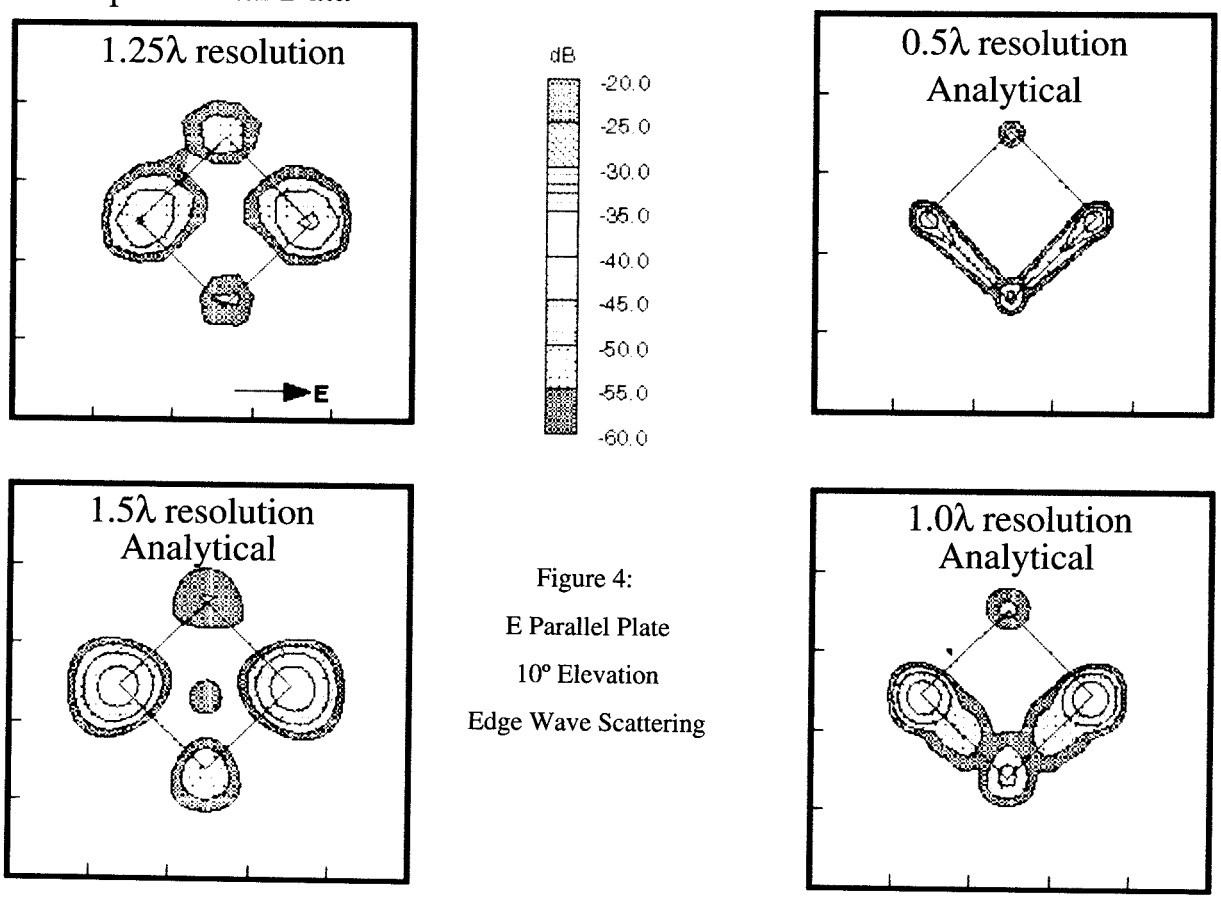

Figure 4:

E Parallel Plate

10° Elevation

Edge Wave Scattering

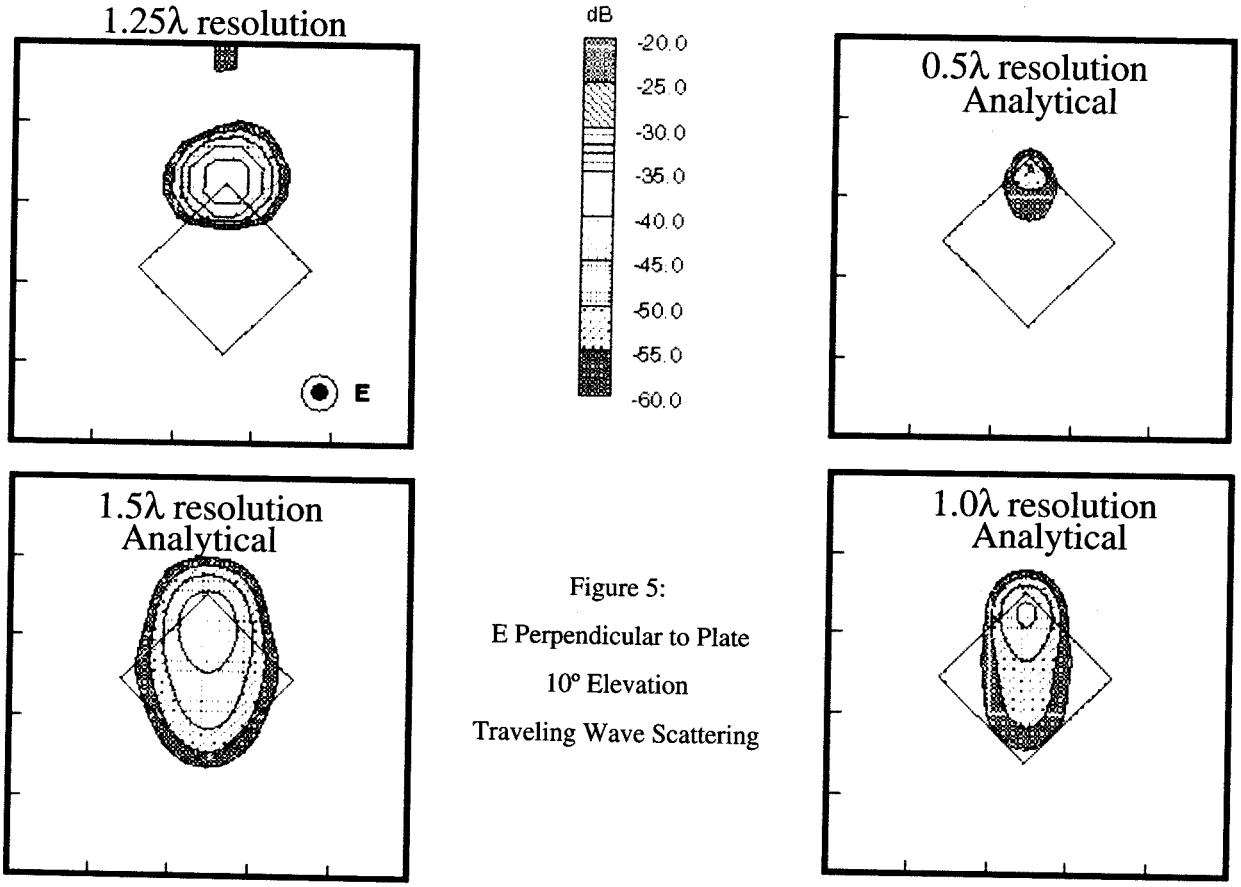

Figure 5:

E Perpendicular to Plate

10° Elevation

Traveling Wave Scattering

Issue	***Bistatic k Space Images***	***Experimental Images***
Origin of scattered field	Bistatic fields computed from generalized radiation integral	Measured backscatter fields
Transform Domain	Directly in k space	Frequency for down range Angle for cross range
Fourier Transform Variables	Wave number k and position r, kr	Frequency and time, ωt for down range and $kr\theta$ for cross range
Target Excitation (What the image represents)	Only at frequency and illumination angle of excitation	Varies over the excitation frequency and illumination angle
Focus/Image Smear	None since image is computed directly in k space on an orthogonal grid of uniformly spaced points	Rotation angle limited to small angle without using focusing algorithms. Inherently a circular region in transform space
Resolution	$\approx\lambda/2$, limited only by granularity of current representation, typically $\approx\lambda/10$, requires twice the experimental bandwidth	Set by available frequency bandwidth and small rotation angle approximation
Time delayed multiple bounce	Images currents which radiate in direction of image	Images downrange as time delay, hence see delayed in time
1-D Images 2-D Images 3-D Images	Down range (radial) in k space add cross range in k space add perpendicular direction in k space	Frequency Sweep add rotation angle add measurements over orthogonal plane
Fidelity for distributed current radiation (traveling waves)	Images the radiation as a distributed source	Because of frequency sweep, images the end points of distributed source
Antenna Images	Straight forward application	???
Image in direction other than excitation, i.e., bistatic images	Straight forward application	Very difficult, seldom done
Cross polarized image	Straight forward application	If separate transmit and receive feeds, rotate one feed

Table I Image Issues for Bistatic k-Space and Experimental